Journal of Photochemistry & Photobiology A: Chemistry 390 (2020) 112299

Contents lists available at ScienceDirect

Journal of Photochemistry & Photobiology A: Chemistry

journal homepage: www.elsevier.com/locate/jphotochem

A bifunctional probe based on naphthalene derivative for absorbance-ratiometic detection of Ag^+ and fluorescence "turn-on" sensing of Zn^{2+} and its practical application in water samples, walnut and living cells

Na-Na Li[a], Cai-Feng Bi[a], Xia Zhang[a], Cun-Gang Xu[a], Chuan-Bin Fan[a], Wei-Song Gao[a], Zi-Ao Zong[b], Shan-Shan Zuo[a], Chuan-Feng Niu[a], Yu-Hua Fan[a,*]

[a] Key Laboratory of Marine Chemistry Theory and Technology, Ministry of Education, College of Chemistry and Chemical Engineering, Ocean University of China, Qingdao, Shandong, 266100, PR China

[b] Schoolof Laboratory Medicine, Youjiang Medical Universityfor Nationalities, Baise, 533000 Guangxi, PR China

ARTICLE INFO

Keywords:
Absorbance-ratiometic
Fluorescence
Ag^+
Zn^{2+}
X-ray crystallography
Cells image

ABSTRACT

In this work, naphthalene with good biocompatibility was selected, and the probe **NBOS** was synthesized with 2-Amino-phenol and 2-Amino-benzenethiol. The structure of probe **NBOS** was confirmed by X-ray Crystallography. Furthermore, the probe showed absorbance-ratiometic sensing for Ag^+ over a pH range from 6 to 7.5 and fluorescence "turn on" signal response towards Zn^{2+} in the pH range of 6–10 in EtOH/H_2O (9/1, V/V, pH = 7.4) mixture. The detection limit was obtained to be 4.24 μM for Ag^+ and 3.17 nM for Zn^{2+}. Moreover, it could be efficiently recycled by treating Na_2EDTA. The sensing mechanism of probe **NBOS** toward Ag^+ and Zn^{2+} was investigated by FT-IR, HNMR, job'plot and ESI-MS. Typically, the coordination mode of **NBOS** with Zn^{2+} was confirmed by DFT calculation. Moreover, probe **NBOS** was successfully applied in the detection Ag^+ and Zn^{2+} in real water samples. Importantly, probe **NBOS** could be used to detect Zn^{2+} in walnut and living cells. Based on the high throughput analysis strategy, absorbance and fluorescence signals of **NBOS** could be designed as a NOT and OR logic gate controlled by Ag^+ (Input 1) and Zn^{2+} (Input 2).

1. Introduction

The detection of heavy and transition metal ions in biological samples was challenging and special attentions had been devoted to Ag^+ and Zn^{2+}. Zinc was an important essential trace element and it played significant roles in many biological processes, such as regulation of metalloenzyme, protein expression and apoptosis [1–3]. However, excess of Zn^{2+} in vivo biology could also cause many illnesses, including Alzheimer's disease, Parkinson's disease, Epilepsy and Ehlers-Danlos syndromeetc [4–6]. Ag^+ was widely used in jewellery, therapeutic and cosmetics [7]. Besides, Ag^+ ion displayed extensive effects on human health including cytotoxicity, failure of several organisms (immunity, nervous, and digestive system) and inhibition of mitochondrial [8,9]. However, Ag^+ and Zn^{2+} caused a lot of serious environmental pollution because of their widespread use in the industry [10–12]. In view of the roles played by Ag^+ and Zn^{2+}, to develop more rapid, sensitive and simple methods for accurate detection of Ag^+ and Zn^{2+} was necessary and important for biological system and environment.

So far, many modern techniques were employed for the detection of Ag^+ and Zn^{2+}, such as atomic absorption spectrometry [13,14], electroanalysis [15] and inductively coupled plasma mass spectrometry [16]. Compared with those detection methods mentioned above, fluorescence probes had attracted attention due to its high sensitivity, simple operation and easy synthesis [17–19]. Therefore, it was used to detect metal ions. A number of probes for the detection Ag^+ and Zn^{2+} had been developed using fluorescent and/or colorimetric methods. Yin's team developed a novel fluorescence probe using terpyridyl triphenylamine derivative, and the probe showed fluorescence turn on response for Zn^{2+} and Cd^{2+} in THF [20]. Das's team synthesized a benzothiazole functionalized probe L1, which exhibited colorimetric as well as fluorometric response to Zn^{2+} in MeOH/H_2O (7/3, V/V, pH = 7.3) buffered solution, but Cd^{2+} also triggered the emission at similai wavelength [21]. Huo etc. team developed a novel fluorescence probe by conjugated with benzimidazole and phenol as a fluorophore, realizing a fluorescent on detection for Zn^{2+} in EtOH [22]. Chen etc. synthesized a new 9,9′-bianthracene-based thiosemicarbazone fluorescence probe, which exhibited a characteristic fluorescence quenching

* Corresponding author.
E-mail address: fanyuhua301@163.com (Y.-H. Fan).

https://doi.org/10.1016/j.jphotochem.2019.112299
Received 16 August 2019; Received in revised form 9 December 2019; Accepted 10 December 2019
Available online 16 December 2019
1010-6030/

phenomenon in the presence of Ag^+ in DMF/H_2O (9/1, V/V, pH = 3.0) [23]. Singh etc. developed a new schiff base probe, which displayed fluorescence turn off response for Ag^+ in CH_3CN/H_2O (1/1, V/V, pH = 7.4) medium [24]. Lin etc. developed a fluorescein spirolactam derivative and used as a turn-on fluorescence probes for the detection of Ag^+ in EtOH/H_2O (1/4, V/V, pH = 9.0) solution [25]. But some of the reported probe for Zn^{2+} still suffer from the shortcomings such as insolubility in water, couldn't detect under physiological condition or interfered by Cd^{2+}. Moreover, most of fluorescence probes for the detection Ag^+ belonged to "on-off" type, which was disadvantageous in most cases. Even though fluorescent turn-on probe was developed, but it showed significant response to Ag^+ in basic medium, which limited their practical applications [25]. UV absorbance-ratiometric probes could conveniently monitor metal ions by the visible range compared to fluorescence probes. So, it was suitable for the detection of Ag^+. Recently, multi-ion responsive probe attracted more interests because their advantages of low cost, higher efficiency, easy sample preparation and time saving. To data, a single probe for the selective detection of Ag^+ and Zn^{2+} has never been reported except the multi-analyte sensor array based on fluorescein designed by Li et al., but the probe was used to detect Ag^+ and Zn^{2+} in different medium, respectively, which caused the complicated preparation process [26]. Hence, there were strong needs in the development of absorbance-ratiometic and fluorescence probes for the detection of Ag^+ and Zn^{2+}.

ESIPT sensing mechanisms had been widely used to design UV absorbance-ratiometric and fluorescence "turn on" probe [27–29]. One-way ESIPT process at the excited state caused fluorescence quenching [30,31]. However, upon addition of metal ions, both ratiometric and fluorescence "turn on" response appeared by broking ESIPT progress. Taking the above statements into consideration, probe **NBOS** was designed and synthesized with 3-hydroxy-2-naphthoic acid, 2-Amino-phenol and 2-Amino-benzenethiol (Scheme1). Hydroxyl, N, S and O creating a multipoint binding pocket, which Ag^+ and Zn^{2+} could coordinate in a cooperative breaking Excited-State Intramolecular Proton Transfer (ESIPT). Probe **NBOS** could detect Ag^+ by absorbance-ratiometic and exhibited high selectivity for Zn^{2+} by fluorescence "turn on" response, especially distinguishing Zn^{2+} from Cd^{2+} in EtOH/H_2O (9/1, V/V, pH = 7.4) mixture. Comparison of the common methods and probe molecules of **NBOS** with the previously reported Ag^+/Zn^{2+} probes were shown in Table 1. Moreover, the sensing mechanism of **NBOS** with Ag^+ and Zn^{2+} were confirmed by FT-IR, HNMR, job'plot, ESI-MS and DFT calculation. The probe **NBOS** was further applied for practical water samples, walnut and could be used in the construction of molecular logic gate. Importantly, fluorescence image of Zn^{2+} in living 293T cells confirmed its value in biological system.

2. Experimental

2.1. General comments

^1H NMR spectra of Compound 2 and **NBOS** were measured on a Bruck AV-600 and AV-500 spectrometer in $CDCl_3$, respectively. The IR spectrum was collected with a Perkin-Elmer IR spectrophotometer using KBr pellet. Pgeneral TU-2550 UV–vis spectrophotometer and Perkin Elmer LS55 fluorescence spectrometer were employed to measure absorption and fluorescence spectra, respectively. Mass spectrum was obtained on an Agilent 6220 Quadruple LC/MS (Agilent Co, USA). X-ray diffraction data were collected on a Bruker Smart CCD X-ray single-crystal diffractometer.

All the materials for synthesis and spectral analysis were of analytical grade or higher, purchased from commercial sources, and used without further purfication. Ultrapure water was used throughout all the expriments. The solution of various mental ions were prepared from $AgNO_3$, KCl, $MgCl_2{\cdot}6H_2O$, $Ba(ClO_4)_2$, $Zn(NO_3)_2{\cdot}6H_2O$, $Cu(NO_3)_2{\cdot}3H_2O$, $Cd(NO_3)_2{\cdot}4H_2O$, $Pb(NO_3)_2$, $CoSO_4{\cdot}7H_2O$, $NiCl_2{\cdot}6H_2O$, $CaCl_2$, $Al(NO_3)_3{\cdot}9H_2O$, $HgCl_2$, Na_2SO_4, $FeCl_2{\cdot}4H_2O$, $FeCl_3{\cdot}6H_2O$, $LiNO_3$, $La(NO_3)_3{\cdot}6H_2O$, $SrCl_2{\cdot}6H_2O$. The pH of **NBOS** solution was adjusted with HCl, NaOH and TRIS aqueous solution. For fluorescence measurements, excitation wavelength was 450 nm and the excitation and emission wavelength band passes were both set at 5 nm and 5 nm.

2.2. Fluorescence quantum yield measurement

The fluorescence quantum yield was calculated according to following equation by selecting rhodamine B (Φ = 0.89 in ethanol) as standard.

$$\Phi_x = \Phi_{st} (A_x/A_{st}) (D_x/D_{st}) (\eta_x/\eta_{st})^2$$

where Φ stands for the fluorescence quantum yield. St subscript denotes the standard and x means sample. A is the absorbance at excitation wavelength, D is the integrated area under the flfluorescence emission spectra, and η is the refractive index of the solvent [32,33].

2.3. X-ray analysis

The structure of **NBOS** was characterized by X-ray crystallographic analysis. **NBOS** (10 mg) was dissolved in 10 mL dichlormethane and petroleum ether (1:1, V/V) mixture, and the solvent was evaporated slowly at room temperature for 2 days to obtain single crystals of **NBOS** suitable for X-ray analysis.

2.4. Synthesis of compound 2

Hydroxy-naphthalene-2-carboxylic acid (1.88 g, 10 mmol) and 2-Amino-phenol (1.09 g, 10 mmol) were dissolved in polyphosphoric acid (PPA, 10 mL) and heated to 180 °C for 3 h with fiercely stirring. After

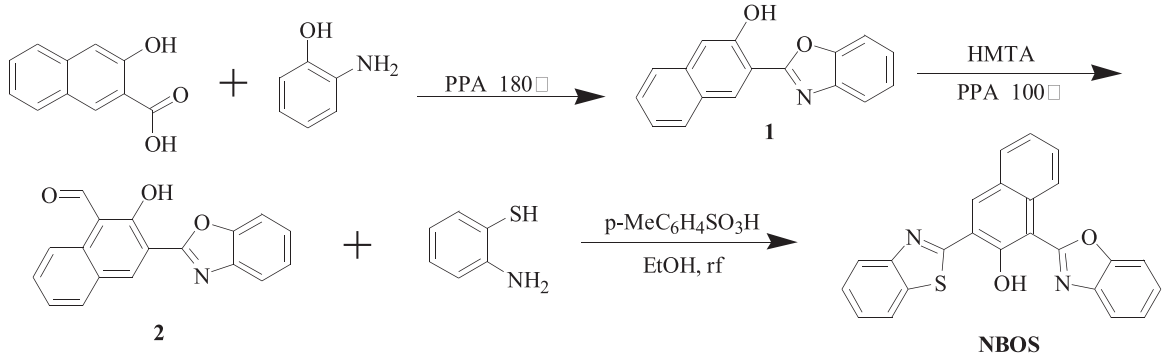

Scheme 1. Synthesis of **NBOS.**

Table 1
Comparison of the common methods and probe molecules of **NBOH** with the previously reported Ag^+/Zn^{2+} probes.

Ref.	probe molecules and synthesi	Methods of detections	Media	LOD
[20]	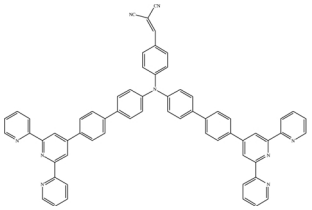	Zn^{2+} Turn on	THF	3.7×10^{-7} M
[21]	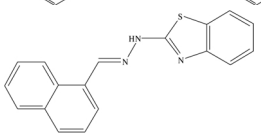	Zn^{2+} colorimetric and fluorometric response	MeOH/H_2O (7/3, V/V, pH 7.3)	6.5×10^{-5} M
[22]	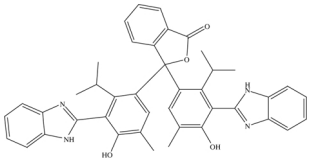	Zn^{2+} Turn on	EtOH	2.5×10^{-5} M
[23]		Ag^+ Turn off	DMF/H_2O (9/1, V/V, pH 3.0)	1.99×10^{-5} M
[24]	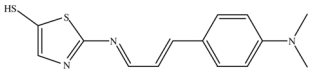	Ag^+ Turn off	CH_3CN/H_2O (1/1, V/V, pH 7.4)	5×10^{-6} M
[25]	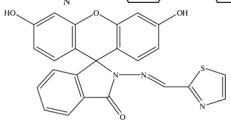	Ag^+ Turn on	EtOH/H_2O (1/4, V/V, pH 9.0)	8×10^{-8} M
[26]	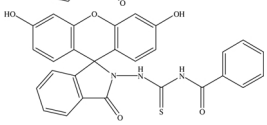	Ag^+ Turn on Zn^{2+} Turn on	Ag^+ EtOH/H_2O (2:8, v/v, pH 7.4) Zn^{2+} CH_3CN/H_2O (2:8,v/v, pH 7.4)	Ag^+ 1×10^{-9} M Zn^{2+} 1×10^{-5} M
	This work	Ag^+ UV-vis ratiometic Zn^{2+} Turn on	EtOH/H_2O (9/1, V/V, pH 7.4)	Ag^+ 4.24×10^{-6} M Zn^{2+} 3.17×10^{-6} M

the reactants were fully consumed (monitored by TLC), the reaction mixture was cooled down to 100 °C. Then HMTA (2.8 g, 20 mmol) was added to the solution obtained above and the mixture was stirred at 100 °C for 5 h and cooled. The reaction mixture was poured in 100 mL of water. The precipitate was filtered, washed with water and dried. The product was purified by silica gel column chromatography (eluent-dichloromethane) and washed with water to give compound 2 (610 mg, 21 %) as green powder [34]. ^{1}H NMR (Fig. S1) (600 MHz, $CDCl_3$) δ 12.58 (s, 1H), 10.97 (s, 1H), 9.13 (s, 1H), 8.73 (s, 1H), 7.80 (d, 1H), 7.72 (d, 1H), 7.62 (q, 2H), 7.40 (m, 3H).

2.5. Synthesis of compound *NBOS*

2-Amino-benzenethiol (125 mg, 1 mmol) and p-$MeC_6H_4SO_3H$ (10 mg, 0.2 mmol) were added into a solution of compound 2 (289 mg, 1 mmol) in EtOH (20 mL). The mixture was stirred for 12 h under reflux conditions. After cooling to room temperature, the precipitate produced was filtered and purified by column chromatography using dichlormethane and petroleum ether (1:1, V/V) to give compound **NBOS** (80 mg, 20 %) as green crystal [35]. ^{1}H NMR (Fig. S2) (500 MHz,$CDCl_3$) ^{1}H NMR (500 MHz, $CDCl_3$) δ 12.20 (s, 1 H), 8.79(s, 1 H), 8.24(d, 1 H), 8.10(d, 1 H), 8.04(d, 1 H), 7.94(d, 1 H), 7.75(d, 1 H), 7.70(d, 1 H), 7.56(m, 2 H), 7.47(m, 4 H). ESI–MS (Fig. S3): calcd for $C_{24}H_{14}N_2O_2S$: 393.07 [**NBOS**-H]$^-$, found: 393.07.

2.6. Synthesis of [*NBOS* + Zn^{2+}] complex

To 10 mL solution of compound **NBOS** (10 mg, 0.025 mmol) in EtOH/CH_2Cl_2 (4:1, V/V), $Zn(NO_3)_2{\cdot}6H_2O$ (7.5 mg, 0.025 mmol) was added and stirred. The end-point of the reaction was confirmed by TLC when the spot of probe **NBOS** was disappeared. The solvent was evaporated at room temperature for 2 days to obtain **NBOS** + Zn^{2+} complex (yellow powder).

2.7. Synthesis of [*NBOS* + Ag^+] complex

The solution of **NBOS** (10 mg, 0.025 mmol) and $AgNO_3$ (10 mg, 0.075 mmol) in 9 mL EtOH and 1 mL H_2O was stirred for 2 days at room temperature and the reaction was monitored by TLC for completion.

2.8. Cell incubation and fluorescence image

293T cells were grown in DMEM medium which supplemented with 10 % (v/v) fetal bovine serum, penicillin (100 μg/mL), and streptomycin (100 μg/mL). The 293T cells were seeded on 8-well plates and incubated 24 h at 37 °C in above culture medium and allowed to grow to 60–70 % confluence. For imaging of Zn^{2+} in living cells, the cells was cultured using fresh medium and the 10 μmol/L probe **NBOS** was added to each well. After being incubated for 30 min, the Zn^{2+} was added into for another 30 min. Fluorescence image of the cells were observed on a confocal laser scanning microscope (Olympus FV1000), with green channal imaging obtained from 500 to 600 nm with 488 nm excitation.

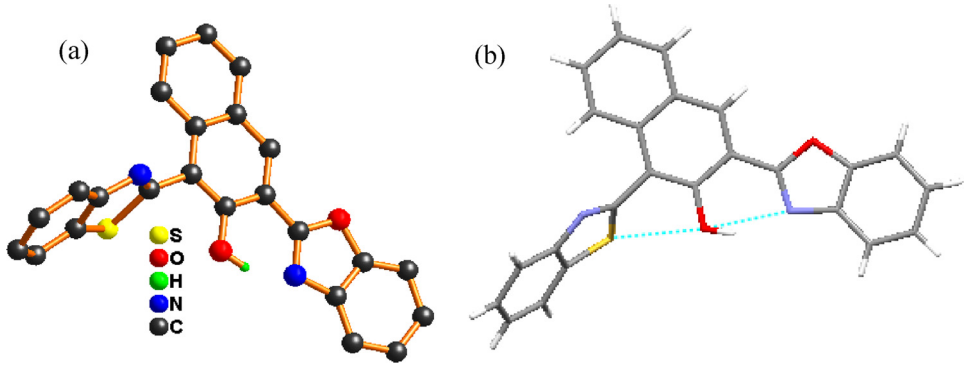

Fig. 1. X-ray crystal structure of **NBOS**.

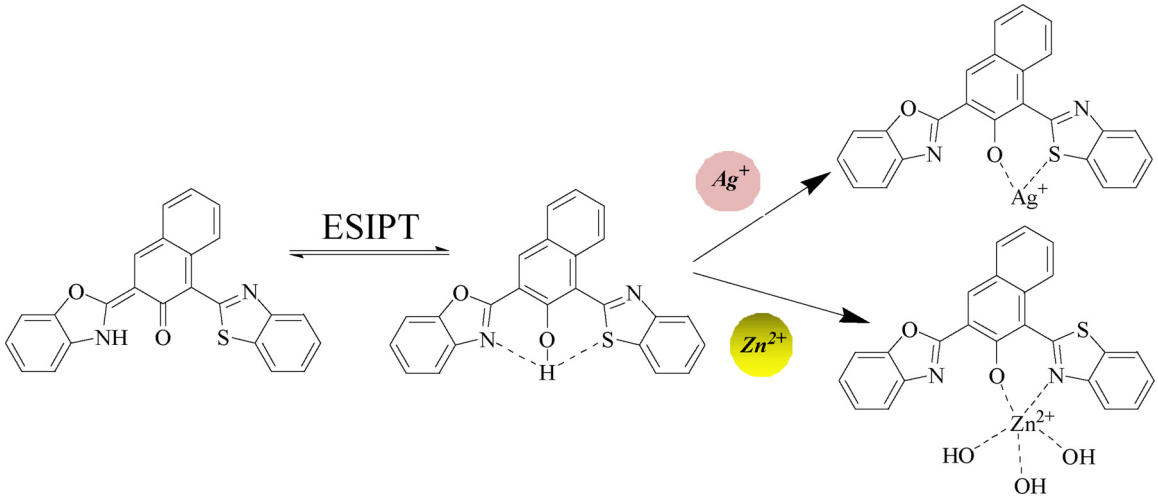

Scheme 2. Proposed sensing mechanism of **NBOS** with Ag^+ and Zn^{2+}.

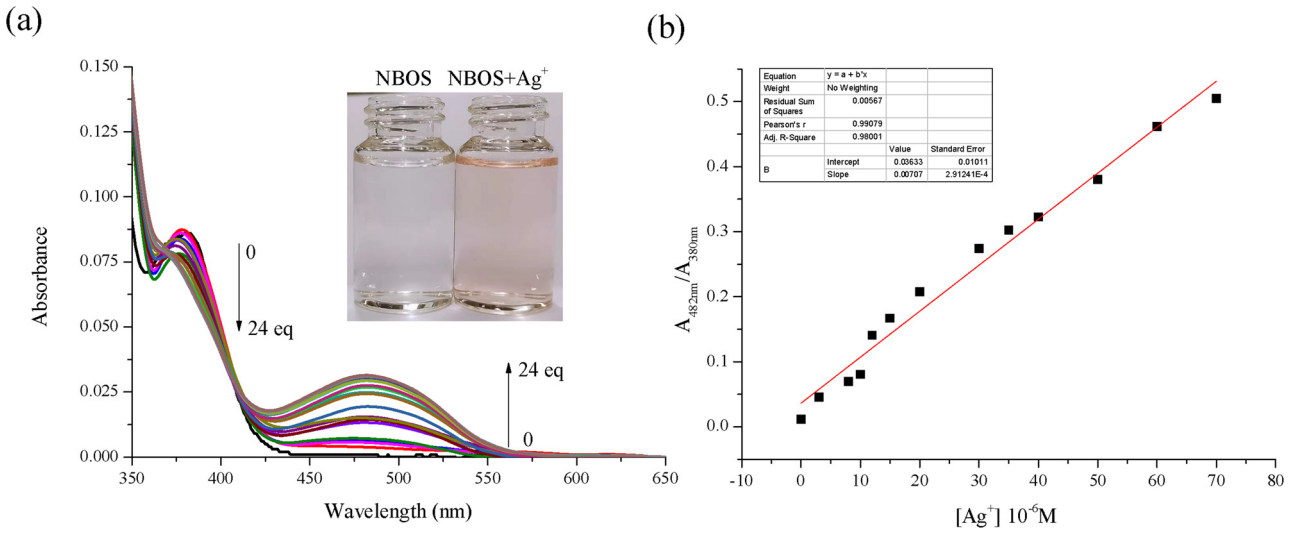

Fig. 2. (a) UV-vis spectral changes of **NBOS** (10 μM) towards different concentrations of Ag^+ in EtOH/H_2O (9/1, V/V, pH = 7.4) medium. Inset: The color change of **NBOS** (20 μM) before and after addition of Ag^+ (50 μM) in EtOH/H_2O (9/1, V/V, pH = 7.4) medium under normal light. (b) The linear responses of UV–vis ratio at 380 nm and 482 nm (A_{482nm}/A_{380nm}) with Ag^+ concentractions.

3. Results and discussion

3.1. Crystallographic details for *NBOS*

The structure of **NBOS** was further confirmed by single crystal X-ray diffraction analysis, which clearly revealed the nonplanar structure of **NBOS** (Fig. 1a). The dihedral angle between the naphthalene and benzooxazole unit and benzothiazole was 63.7° (Fig. S4). The severe distortion of **NBOS** may be ascribed to the steric hindrance effect. The molecular structure of **NBOS** was stabilized by intramolecular hydrogen bonding which was clearly visible in Fig. 1b. The intramolecular hydrogen bond was formed between O—H of naphthalene ring, N atom of

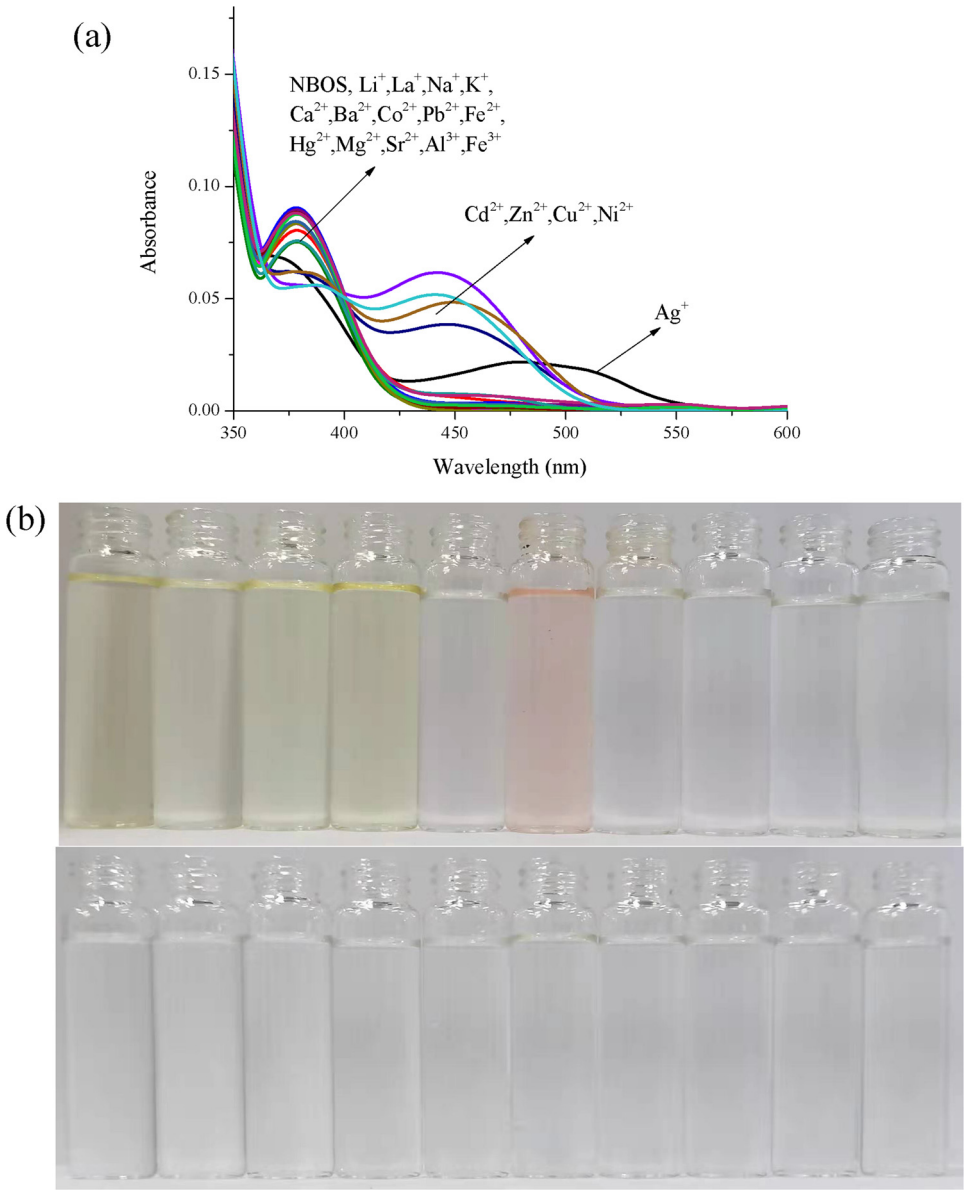

Fig. 3. (a) UV-absorbance spectra of **NBOS** (10 μM) in the presence of various metal ions (50 μM) in EtOH/H_2O (9/1, V/V, pH = 7.4) medium. (b) Color change induced after addition of 5 equiv. of various metal ions (Zn^{2+}, Ni^{2+}, Cd^{2+}, Cu^{2+}, **NBOS**, Ag^+, Co^{2+}, Mg^{2+}, Ca^{2+}, Ba^{2+}, Hg^{2+}, Pb^{2+}, Sr^{2+}, Fe^{2+}, Al^{3+}, Fe^{3+}, Li^+, La^+, Na^+, K^+) to **NBOS** (20 μM) in EtOH/H_2O (9/1, V/V, pH = 7.4) medium.

benzooxazole and S atom of benzothiazole preferentially, which was necessary for occurrence of the desired ESIPT process. Furthermore, due to the coplanar of naphthalene and benzooxazole, the proton would hop between hydroxy of naphthalene ring and imine of benzooxazole at excited state preferentially, the so-called ESIPT process (Scheme 2). All the significant crystallographic data and refinement parameters were shown in Tables S1 and S2.

3.2. UV–vis absorbance-ratiometic detection of Ag^+

The investigation of probe **NBOS** sensing ability was carried out by UV–vis absorbance titrations (Fig. 2) in EtOH/H_2O (9/1, V/V, pH = 7.4) mixture. The absorption maximum of probe **NBOS** was 380 nm. With gradual addition of Ag^+, the origin absorption band at 380 nm decreased gradually while a new absorption band at 482 nm increased accompanied by a visual color change from colourless to pale yellow. A well-defined isosbestic point was observed at 396 nm, indicating that only one new species was fomed, supporting the assumption that **NBOS** and **NBOS** + Ag^+ were coexisting in the solution [36]. Obviously, the UV–vis titration experiments exhibited that the UV–vis ratio at 380 nm and 482 nm ($A_{482\,nm}/A_{380\,nm}$) increased from 0.1 to 1.8. In addition, the UV–vis ratio at 368 nm and 442 nm ($A_{442\,nm}/A_{368\,nm}$) was plotted as a function of the various concentration Ag^+ added. The good linearity between UV–vis ratio of $A_{482\,nm}/A_{380\,nm}$ and Ag^+ concentrations ranging from 3 μM to 80 μM were observed and the detection limit was obtained to be 4.24 μM by applying equation 3 δ/S [37].

The selectivity of probe **NBOS** for Ag^+ was investigated by UV–vis absorbance spectrometry in EtOH/H_2O (9/1, V/V, pH = 7.4) mixture. In Fig. 3, probe **NBOS** exhibited major absorption peak at 380 nm. Addition Zn^{2+}, Cd^{2+}, Cu^{2+}, Ni^{2+} red shifted the absorbance peak from 380 nm to 440 nm and resulted in slightly yellow green color appearance. However, addition of Ag^+ showed the reduction of origin absorption band at 380 nm and appeared a new absorption band at 482 nm. Such a large red shift in absorption spectrum lead to an obvious color change from colourless to pale pink. These phenomena

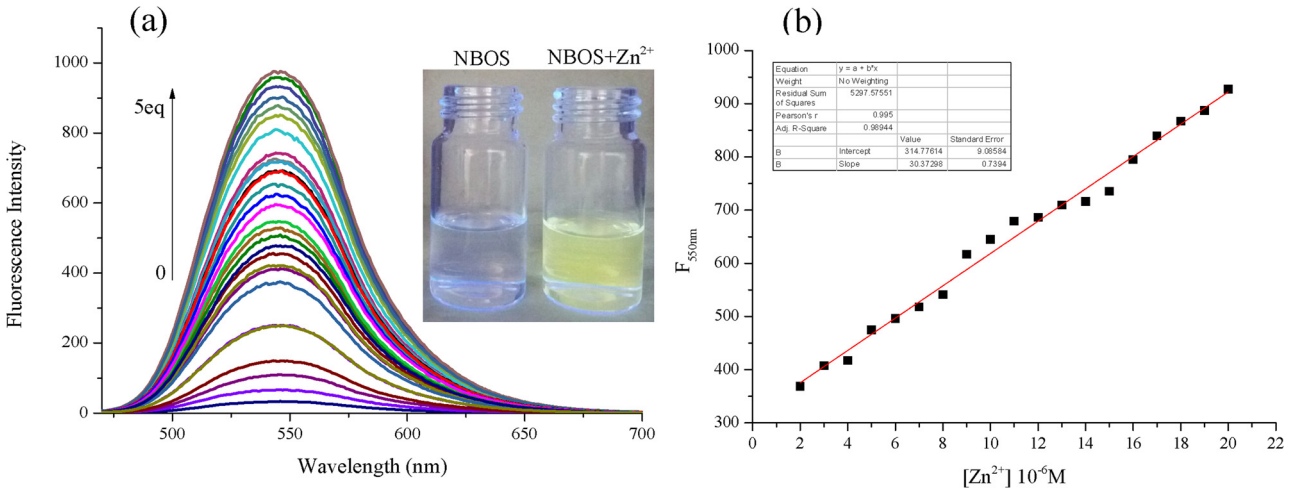

Fig. 4. (a) Fluorescence spectral changes of **NBOS** (10 μM) towards different concentrations of Zn^{2+} in EtOH/H_2O (9/1, V/V, pH = 7.4) medium. Inset: Photograph of the fluorescence change of the solution of **NBOS** (10 μM) before and after addition of Zn^{2+} (50 μM) in EtOH/H_2O (9/1, V/V, pH = 7.4) medium under UV light of 365 nm. (b) The linear responses of fluorescence intensity at 550 nm with Zn^{2+} concentractions.

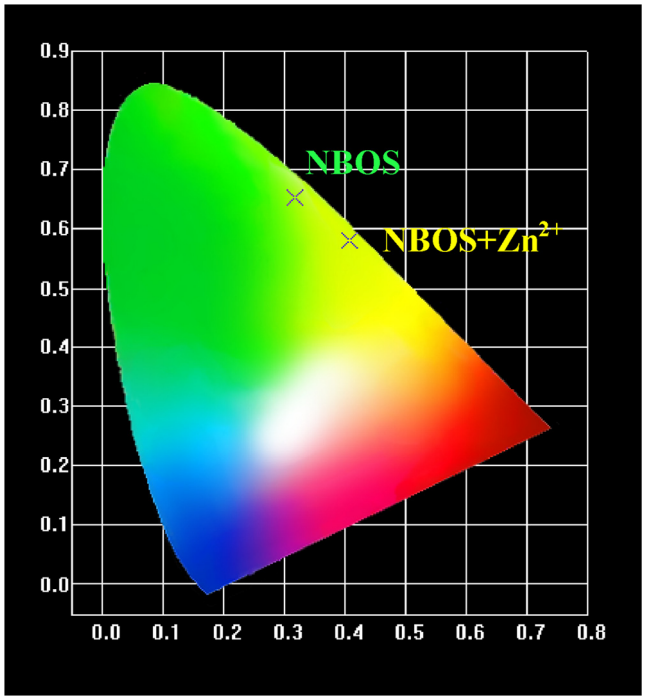

Fig. 5. CIE diagram of the probe **NBOS** and **NBOS** with Zn^{2+} (5 equiv.) in EtOH/H_2O (9/1, V/V, pH = 7.4) medium (λ_{ex} = 450 nm).

suggested that **NBOS** could be used as a Ag^+ probe. But, when Zn^{2+}, Cd^{2+}, Cu^{2+} and Ni^{2+} were present, the detection of Ag^+ almost certainly interfere.

Furthermore, the effect of pH on the UV–vis ratio sensing ability of **NBOS** towards Ag^+ was investigated. Probe **NBOS** exhibited negligible relative absorbance ratios at 482 nm and 380 nm ($A_{482\,nm}/A_{380\,nm}$) over a wide pH range (2–10). Upon addition of Ag^+, a remarkable increase of absorbance ratios ($A_{482\,nm}/A_{380\,nm}$) in the pH range from 6 to 7.5 (Fig. S5). Hence, the suitable pH range of 6–7.5 made it possible to detect Ag^+ using probe **NBOS**.

3.3. Fluorescence titration spectra for Zn^{2+}

Moreover, as shown in Fig. 4, upon addition of Zn^{2+}, the fluorescence intensity at 550 nm increased gradually, and probe **NBOS** with

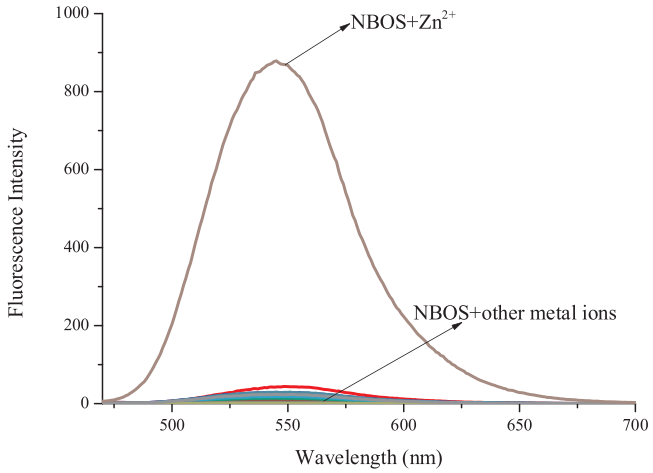

Fig. 6. Fluorescence spectral of **NBOS** (10 μM) in the presence of various metal ions (50 μM) in EtOH/H_2O (9/1, V/V, pH = 7.4) medium (λ_{ex} = 450 nm).

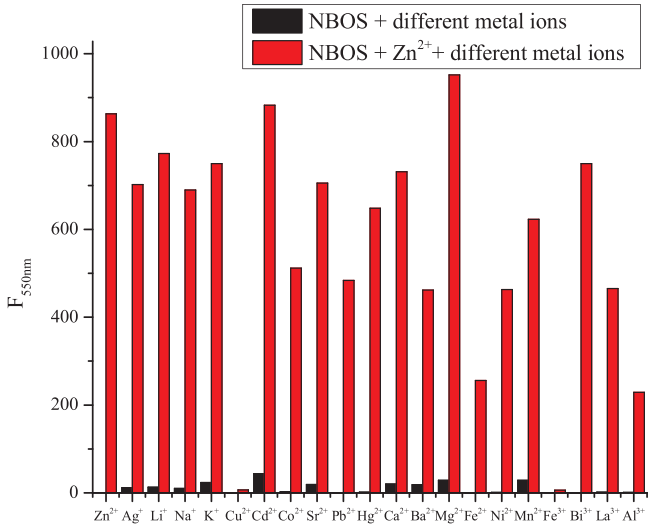

Fig. 7. Fluorescence intensity at 550 nm of **NBOS** (10 μM) upon addition of various metal ions (50 μM) in the presence Zn^{2+} (50 μM) in EtOH/H_2O (9/1, V/V, pH = 7.4) mixture (λ_{ex} = 450 nm).

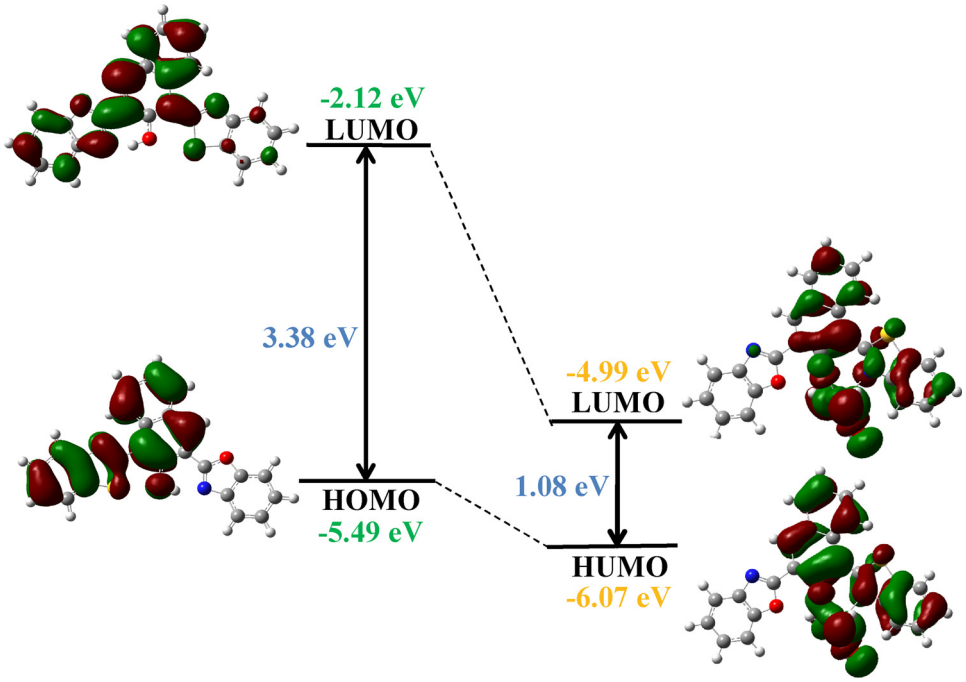

Fig. 8. The calculated molecular orbitals and the HOMO-LUMO gaps of **NBOS** and **NBOS** + Zn^{2+}.

Zn^{2+} showed visual color change from colorless to yellow under 365 nm UV lamp. Furthermore, there was a good linear relationship between the maximal fluorescence intensity of **NBOS** and the concentration of Zn^{2+} varied from 2 μM to 20 μM. The detection limits of probe **NBOS** for Zn^{2+} was confirmed to be 3.17×10^{-9} M by applying equation 3 δ/*S* [37]. The nonfluorescent nature of the probe **NBOS** was caused by the ESIPT progress at the excited state. Because of chelating of the probe **NBOS** with Zn^{2+}, the ESIPT processes in corresponding were inhibited, resulting in significant enhancement of the fluorescence.

CIE chromaticity diagram was usually used to better explain the colour variation in the emission spectrum of luminescent materials [38,39]. To better understand chromaticity changes of the probe upon complexation, CIE chromaticity coordinates were also calculated from the fluorescence spectrum. The CIE system identified the colour of the fluorescent emission more precisely by a two-dimensional space (XY plane). The CIE chromaticity coordinates of **NBOS**-Zn^{2+} complex was found to be x = 0.4084, y = 0.5792 at room temperature. These color point data suggested that the color coordinates shifts gradually from yellowwish green to yellowgreen color region upon progressive addition of Zn^{2+} in to the solution of probe **NBOS** (Fig. 5).

To investigate selectivity of probe **NBOS**, it was incubated with each of various metal ions including Ag^{+}, Cd^{2+}, Co^{2+},Na^{+}, K^{+}, Ba^{2+}, Fe^{2+} Co^{2+}, Ni^{2+}, Ca^{2+}, Zn^{2+}, Cd^{2+}, Cu^{2+}, Mg^{2+}, Pb^{2+}, Fe^{3+}, Li^{+}, La^{+}, Sr^{3+} and the fluorescence spectroscopy was measured. As shown in Fig. 6, probe **NBOS** alone and other metal ions all exhibited very weak single fluorescence emisson band at 550 nm except for Zn^{2+}. After addition of Zn^{2+}, probe **NBOS** showed a prominent fluorescence enhancement. In addition, the fluorescence quantum yield of probe **NBOS** before and after addition of Zn^{2+} was determined to be as high as 0.03 and 0.62 (using rhodamine B as standard), respectively. This property indicated that probe **NBOS** could specifically fluorescence "turn on" test Zn^{2+}.

Additionally, the competition experiments were performed by adding 5 equiv. Zn^{2+} to the solution of probe **NBOS** in the presence of 5 equiv. above metal ions. As shown in Fig. 7, negligible interference was observed for the detection of Zn^{2+} in the presence of Cd^{2+}, Co^{2+}, Na^{+}, K^{+}, Ba^{2+}, Co^{2+}, Ni^{2+}, Ca^{2+}, Mn^{2+}, Mg^{2+}, Pb^{2+}, Bi^{3+}, Li^{+}, La^{3+}, Sr^{2+}. The probe **NBOS** responses to Zn^{2+} in the presence of Al^{3+} and Fe^{2+} were low but detectable. The fluorescence of **NBOS** + Zn^{2+} complexation was completely quenched by Cu^{2+} and Fe^{3+}. Therefore, **NBOS** could be applied as an effective probe for Zn^{2+} in the presence of most competing metal ions.

The time response of probe represented the sensitivity. Therefore, we further investigated the time response on fluorescence intensity of the probe **NBOS** to Zn^{2+} (2.0 equiv) in EtOH/H_2O (9/1, V/V, pH = 7.4) mixture. The fluorescence response signal showed instant enhancement and reached saturation with 2 s upon addition of Zn^{2+} (Fig. S6). In addition, the fluorescence intensity was almost unchanged over a period of time, indicating that complexation process of probe **NBOS** with Zn^{2+} was fast and stable, which had potential application for quickly detection Zn^{2+}.

In order to demonstrate whether probe **NBOS** had a good performance under physiological conditions, the pH effect of on the fluorescence and UV–vis response of probe **NBOS** toward Zn^{2+} in a pH range from 2.0 to 12.0 was investigated. As shown in Fig. 8, probe **NBOS** exhibited negligible relative fluorescence intensity at 550 nm over a wide pH range (2–10) (Fig. S7). For the mixture of probe **NBOS** with Zn^{2+}, a strong fluorescence emission at 550 nm was observed in a wide pH range from 6.0 to 10.0, indicating that probe **NBOS** could detect Zn^{2+} under physiological condition.

3.4. Mechanism study

In order to explore the combination code of the probe **NBOS** with Ag^{+} and Zn^{2+}, the FT-IR (Fig. S8), ^{1}H NMR (Fig. S9) of **NBOS** + Ag^{+} and **NBOS** + Zn^{2+} complex were measured. The FT-IR spectra of **NBOS** + Zn^{2+} complex exhibited a wide peak at 3376 cm^{-1}, because of presence of H_2O molecules in the complex. The FT-IR spectra of **NBOS** + Ag^{+} and **NBOS** + Zn^{2+} complex appeared obviously strong peaks at 1350 cm^{-1} and 1381 cm^{-1} respectively, which attributed to N—O vibration of the NO^{3-}. Compared to the FT-IR spectra of **NBOS**, the characteristic —C—S— absorption peak at 1153 cm^{-1} widen and shifted to the lower wavenumber in the presence of Ag^{+} and Zn^{2+}, indicating that the intramolecular hydrogen bond was broken.

^{1}H NMR experiments was performed in $CDCl_3$. The hydroxyl proton of the naphthalene ring part was not observed in the spectrum of **NBOS** + Ag^{+} and **NBOS** + Zn^{2+} complex, suggested the occurrence of

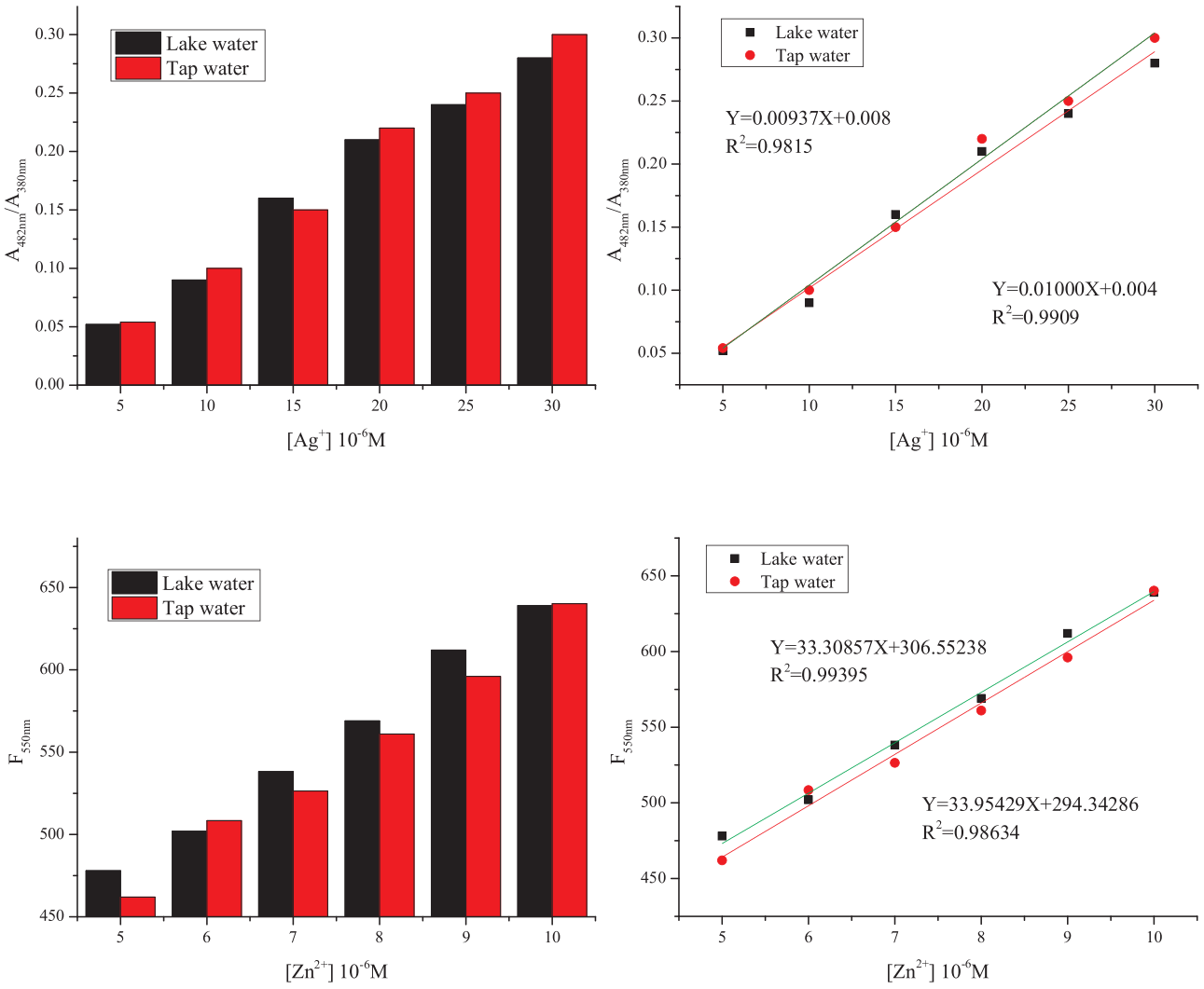

Fig. 9. UV–vis ratio detection of Ag^+ and fluorescence determination of Zn^{2+} in distilled water and lake water by **NBOS** (10 μM) in EtOH/H_2O (9/1, V/V, pH = 7.4) mixture.

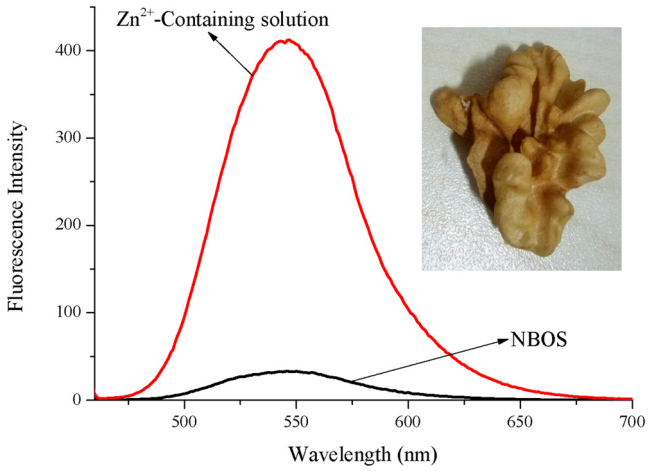

Fig. 10. Fluorescence spectra of **NBOS** (10 μM) for determination Zn^{2+} in walnut in EtOH/H_2O (9/1, V/V, pH = 7.4) mixture.

deprotonation during the coordination of the hydroxyl group with Ag^+/Zn^{2+}. All signal of aromatic protons in the spectrum of **NBOS** + Ag^+ and **NBOS** + Zn^{2+} complex were observed to be decreased and shifted a little downfield as compared to the spectrum of free **NBOS**. This result suggested certain complex formation of **NBOS** and Ag^+/Zn^{2+}.

The detailed binding mode was confirmed by mass spectrometry analysis. The mass spectrum was measured in the presence of Ag^+/Zn^{2+} in EtOH/H_2O (9/1, V/V, pH = 7.4) mixture. The peak at 538.43 was observed, assigned as [**NBOS-H** + Ag^+ + K]$^+$ (calc = 538.9) (Fig. S10), providing a powerful evidence for formation of 1:1 coordination complex between Ag^+ and **NBOS**. The peak at *m/z* 393.07 and *m/z* 254.02 corresponding to [**NBOS**-H]$^-$ (calc = 393.07) and [1/2(**NBOS**-H + Zn^{2+} + 3OH^-)]$^-$ (calc = 254.00) (Fig. S11), respectively, indicating **NBOS** + Zn^{2+} comprised by a receptor, a Zn^{2+} and 3 OH^-. Moreover, the job't plot of the probe **NBOS** with Ag^+ and Zn^{2+} was carried in EtOH/H_2O (9/1, V/V, pH = 7.4) mixture, respectively. The total concentration remained unchanged of **NBOS** + Ag^+ (5×10^{-5} mol/L) and **NBOS** + Zn^{2+} (10^{-5} mol/L) with the molar ratio of Ag^+/Zn^{2+} varied from 0.1 to 0.9 (Fig. S12). Both maximum absorbance ratios ($A_{482\,nm}/A_{380\,nm}$) and fluorescent intensity at 550 nm exhibited at around 0.5 M fraction, suggesting a 1:1 ratio for the probe **NBOS** with Ag^+/Zn^{2+}, which was consistent with the result of mass analysis. According to the UV–vis/fluorescence titration data and 1:1 binding stoichiometry, the association constant (K) of probe **NBOS** with Ag^+/Zn^{2+} was determined by using Benesi-Hildebrand (B–H) equation (Fig. S13) [18,40]. The K value was calculated to be 1.81×10^4 M^{-1} and 9.62×10^4 M^{-1} by curves of [1/(A − A_{min})] against 1/[Ag^+] and 1/

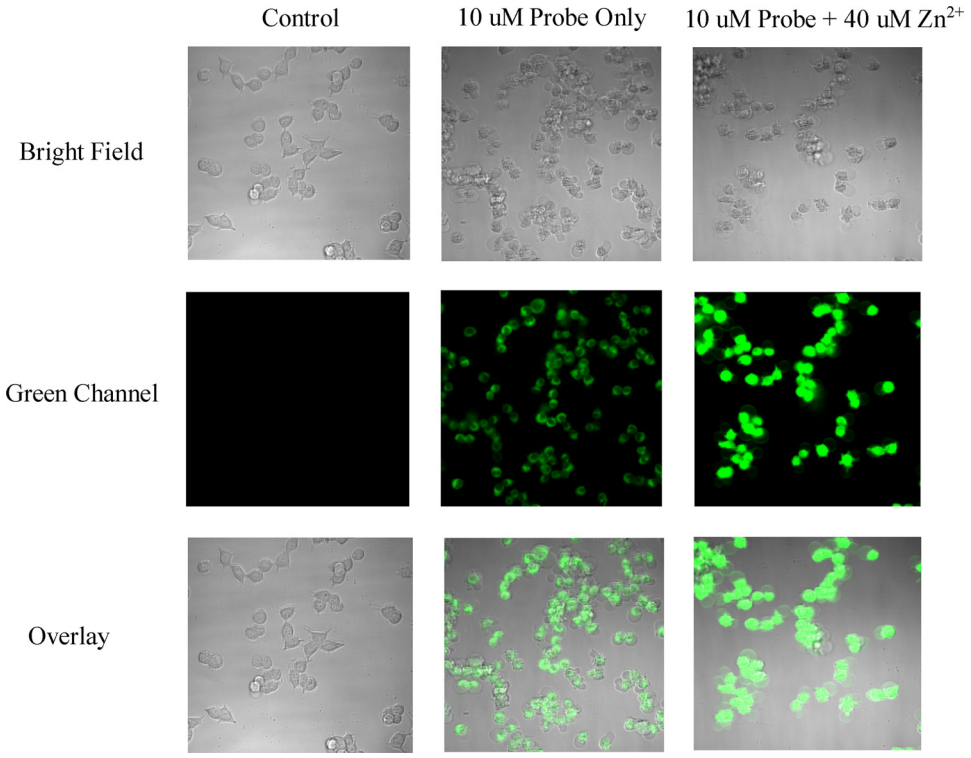

Fig. 11. Fluorescence image of Zn^{2+} in 293T cells.

Input 1	Input 2	Output 1	Output 2
Ag^{+}	Zn^{2+}	$A_{482\ nm}$	$I_{f\,550\ nm}$
0	0	0	0
1	0	1	0
0	1	0	1
1	1	1	1

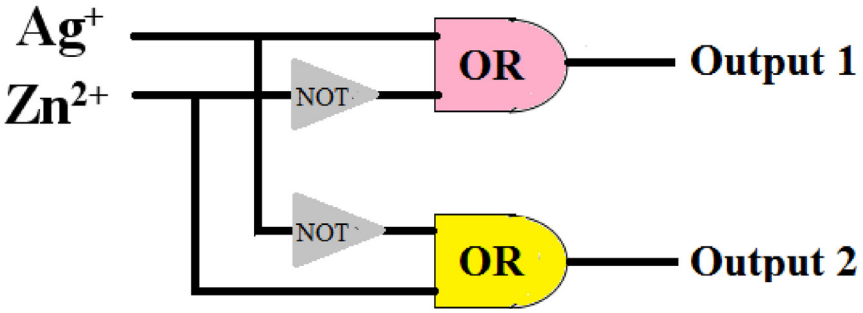

Scheme 3. Truth table and logic gate diagram based on Ag^{+} and Zn^{2+} by means of absorbance and fluorescence intensity.

($F_{550\ nm} - F_{min}$) against $1/[Zn^{2+}]$, respectively.

Based on above experimental supports from various spectroscopic techniques, the proposed mechanism for the detection of Ag^{+}/Zn^{2+} using the probe **NBOS** was well presented in Scheme 2.

3.5. DFT study

To further understand the electronic structures of **NBOS** and **NBOS** $+Zn^{2+}$ complex, density functional theory (DFT) calculation using Gaussian 09 programme was performed [41,42]. As shown in Fig. 8, the

electron cloud in HOMO (−5.49 eV) of **NBOS** was spread on the benzothiazole and naphthalene subunit. The result suggested that hydroxyl and nitrogen atom were likely to chelate with metal ions. Furthermore, the calculated energy gaps between HOMO and LUMO were 3.38 eV for **NBOS** and 1.08 eV for **NBOS** + Zn^{2+}, which suggested the higher stability of **NBOS** + Zn^{2+} than the free **NBOS**. As we expected, the experimental results agree with that of theoretical calculation.

3.6. Reversibility of *NBOS* for Ag^+ and Zn^{2+}

The reversibility was crucial for cost efficiencies of the probe. Therefore, we designed experiments to improve the reversibility of probe **NBOS** to Ag^+ and Zn^{2+} in EtOH/H_2O (9/1, V/V, pH = 7.4) mixture using ethylenediaminetetraacetic acid (Na_2EDTA) as a powerful chelator for metal ions. Upon addition of Na_2EDTA, the UV–vis absorbance spectra of **NBOS** + Ag^+ and fluorescence spectra of **NBOS** + Zn^{2+} almost back to the state of free **NBOS** (Figs. S14 and S15). These results suggested that **NBOS** could serve as a reversible probe for detection Ag^+ and Zn^{2+} in physiological condition.

3.7. Detection Ag^+ and Zn^{2+} in water samples

Considering the pollution of Ag^+ and Zn^{2+} in the environment, the probe **NBOS** was applied in the detection of Ag^+ and Zn^{2+} in real water samples by the proposed UV–vis ratio and fluorimetric method, respectively. The tap water was collected from chemistry building in Ocean university of China. The lake water was collected from lake that located in Ocean university of China. These water samples were spiked with Ag^+ (5, 10, 15, 20, 25, 30 μM) and Zn^{2+} (5, 6, 7, 8, 9, 10 μM), respectively. As shown in Fig. 9, the relative absorbance ratios at 482 nm and 380 nm ($A_{482\,nm}/A_{380\,nm}$) and fluorescence intensity at 550 nm showed nice linearity for tap and lake water. In addition, it displayed good recovery values (97–104 %) (Table S1). These results further indicated that the practical value of the probe **NBOS** for detection Ag^+ and Zn^{2+} in environment. These results suggested that **NBOS** could be used for the detection Ag^+ and Zn^{2+} accurately in real water samples.

3.8. Detection Zn^{2+} in walnut

In order to evaluate the practical application of probe **NBOS** for detection Zn^{2+} in our daily life, the walnut containing trace amount of Zn^{2+} was used in the sample analysis. The walnut (0.5 g) were broke and immersed in HNO_3 (10 mL), then added NaOH and al Zn^{2+}-containing solution [43–45]. In Fig. 10, the probe **NBOS** (5 mL) showed fluorescence enhancement at 550 nm after addition of Zn^{2+}-containing solution (800 μL). According to the linear relationship equation (Y = 21.9030X + 288.3448) obtained in Fig. 10, the Zn^{2+} concentration of Zn^{2+}-containing solution was calculated as 2.6 μmol/L, which revealed that Zn^{2+} content in walnut was 0.0211 mg/g. The result was within the allowable error range contrast to the reported content 0.02 mg/g. These phenomena indicated that probe **NBOS** were convenient and sensitive for the detection Zn^{2+} in walnut.

3.9. Fluorescence image in living cells

We then demonstrated the biological application of probe **NBOS**. In Fig. 11, when 293T cells were treated with probe **NBOS** for 30 min, 293T cells exhibited were green fluorescence in the green channel under fluorescence microscopy. However, after Zn^{2+} was added into the above system for 30 min, the 293T cells showed obvious green fluorescence because of the coordination of probe **NBOS** with Zn^{2+}. Therefore, these results showed that probe **NBOS** could be used for tracking Zn^{2+} in living cells.

3.10. Logic gate

Absorbance peak at 482 nm appeared only occurring coordination between **NBOS** and Ag^+. The fluorescence intensity at 550 nm of probe **NBOS** increased only after addition of Zn^{2+}. Therefore, when we considered the absorbance at 482 nm and fluorescence intensity at 550 nm as outputs, the two signals were Input 1 (Ag^+) and Input 2 (Zn^{2+}), OR and INHIBIT logic gate was constructed [46,47]. When Input 1 (Ag^+) was present and Input 2 (Zn^{2+}) was absent or Input 1 (Ag^+) was absent and Input 2 (Zn^{2+}) was present, the output 2 and output 1 respectively were 0 state, which presented combination gate (blue period). When the opposite situation appeared, it exhibited OR gate (gray period). The logic gate was showed in Scheme 3.

4. Conclusion

In summary, a novel naphthalene based probe **NBOS** for detection Ag^+ and Zn^{2+} by using two different optical modes in EtOH/H_2O (9/1, V/V, pH = 7.4) medium based on the inhibition of ESIPT progress was developed. The binging mode of **NBOS** with Ag^+ and Zn^{2+} was confirmed. Moreover, probe **NBOS** was successfully applied in real water samples detection Ag^+ and Zn^{2+} with good accuracy and exhibited a logic gate with two inputs Ag^+ and Zn^{2+}. Importantly, probe NBOS could be used to detect Zn^{2+} in walnut and living cells.

CRediT authorship contribution statement

Na-Na Li: Conceptualization, Methodology, Software, Data curation, Writing - original draft. **Cai-Feng Bi:** Supervision. **Xia Zhang:** Supervision. **Cun-Gang Xu:** Software, Validation. **Chuan-Bin Fan:** Writing - review & editing. **Wei-Song Gao:** Software, Validation. **Zi-Ao Zong:** Software, Validation. **Shan-Shan Zuo:** Investigation. **Chuan-Feng Niu:** Investigation. **Yu-Hua Fan:** Supervision.

Acknowledgements

This work was supported by the Fundamental Research Funds for the Central Universities (No. 201822012), the National Natural Science Foundation of China (Nos. 21476218 and 21601171).

Appendix A. Supplementary data

Supplementary material related to this article can be found, in the online version, at doi:https://doi.org/10.1016/j.jphotochem.2019.112299.

References

[1] J.X. Fu, Y.X. Chang, B. Li, X.H. Wang, X.M. Xie, K.X. Xu, A dual fluorescence probe for Zn^{2+} and Al^{3+} through differentially response and bioimaging in living cells, Spectrochim. Acta A 225 (2020) 117493.
[2] Z.J. Hu, G.Q. Yang, J.W. Hu, H. Wang, P. Eriksson, R.L. Zhang, et al., Real-time visualizing the regulation of reactive oxygen species on Zn^{2+} release in cellular lysosome by a specific fluorescent probe, Sens. Actuators B: Chem. 264 (2018) 419–425.
[3] Y.T. Shang, S.W. Zheng, M. Tsakama, M. Wang, W.H. Chen, A water-soluble, small molecular fluorescence probe based on 2-(20-hydroxyphenyl) benzoxazole for Zn^{2+} in plants, Tetrahedron Lett. 59 (2018) 4003–4007.
[4] H.H. Song, Z. Zhang, A quinoline-based ratiometric fluorescent probe for discriminative detection of Zn^{2+} and Cd^{2+} with different binding modes, and its Zn^{2+} complex for relay sensing of pyrophosphate and adenosine triphosphate, Dyes Pigm. 165 (2019) 172–181.
[5] S.A. Yoon, J.J. Lee, M.H. Lee, A ratiometric fluorescent probe for Zn^{2+} based on pyrene-appended naphthalimide-dipicolylamine, Sens. Actuators B: Chem. 258 (2018) 50–55.
[6] X.Y. Wen, Q. Wang, Z.F. Fang, An active fluorescent probe based on aggregation-induced emission for intracellular bioimaging of Zn^{2+} and tracking of interactions with single-stranded DNA, Anal. Chim. Acta 1013 (2018) 79–86.
[7] M.L. Desai, H. Basu, B.K. Singhal, S. Saha, S.K. Kailasa, Ultra-small two dimensional MXene nanosheets for selective and sensitive fluorescence detection of Ag^+ and Mn^{2+} ions, Colloids Surf. A 565 (2019) 70–77.

[8] H.Y. Tang, Y. Gao, B. Li, C.W. Li, Y. Guo, Reaction-based colorimetric and ratiometric fluorescent probe for highly selective detection of silver ions, Sens. Actuator B: Chem. 270 (2018) 562-569-55.

[9] D.S. Lin, J.P. Lai, H. Sun, Z. Yang, Y. Zuo, A turn-on fluorescein spirolactam derivative as a high selective fluorescence probe for detection of silver ion(I) in water, Anal. Methods 270 (2018) 562–569.

[10] Y.B. Jiang, C. Gao, X. Zhang, J.S. Yao, Q.Z. Liu, X.X. Cai, A highly selective and sensitive fluorescence probe with A-π-D-π-A structure for detection of Ag+, J. Mol. Liq. Struct. 1163 (2018) 33–40.

[11] H.P. Wang, T.T. Kang, X.J. Wang, L.H. Feng, A facile strategy for achieving high selective Zn(II) fluorescence probe by regulating the solvent polarity, Talanta 184 (2018) 7–14.

[12] X.J. Tian, X.F. Guo, F.S. Yu, L.Y. Jia, An oxalamidoquinoline-based fluorescent sensor for selective detection of Zn^{2+} in solution and living cells and its logic gate behavior, Sens. Actuators B: Chem. 232 (2016) 181–187.

[13] A. Chatterjee, M. Santra, N. Won, S. Kim, J.K. Kim, S.B. Kim, K.H. Ahn, Selective fluorogenic and chromogenic probe for detection of silver ions and silver nanoparticles in aqueous media, Sens. J. Am. Chem. Soc. 131 (2009) 2040–2041.

[14] M. Rajabi, S. Asemipour, B. Barfi, M.R. Jamali, M. Behzad, Ultrasound-assisted ionic liquid based dispersive liquid-liquid microextraction and flame atomic absorption spectrometry of cobalt, copper, and zinc in environmental water samples, J. Mol. Liq. 194 (2014) 166–171.

[15] T. Liu, J. Yin, Y.H. Wang, P. Miao, Construction of a specific binding peptide based electrochemical approach for sensitive detection of Zn^{2+}, J. Electroanal. Chem. 783 (2016) 304–307.

[16] P.A. Panchenko, A.S. Polyakova, Y.V. Fedorov, O.A. Fedorova, Chemoselective detection of Ag^{+} in purely aqueous solution using fluorescence 'turn-on' probe based on crown-containing 4-methoxy-1,8-naphthalimide, Mendeleev Commun. 29 (2019) 155–157.

[17] P. Qu, X.H. Ma, W.S. Chen, D.D. Zhu, H.F. Bai, X.H. Wen, S. Chen, M.T. Xu, A coumarin-based fluorescent probe for ratiometric detection of hydrazine and its application in living cells, Spectrochim. Acta A 210 (2019) 381–386.

[18] X. Yuan, T.H. Leng, Z.Q. Guo, C.Y. Wang, J.Z. Li, W.W. Yang, W.H. Zhu, A FRET-based dual-channel turn-on fluorescence probe for the detection of Hg^{2+} in living cells, Dyes Pigm. 161 (2019) 403–410.

[19] Z. Liu, G.P. Li, Y. Wang, J.L. Li, Y. Mi, D.P. Zou, D.P. Li, Y.J. Wu, Quinoline-based ratiometric fluorescent probe for detection of physiological pH changes in aqueous solution and living cells, Talanta 192 (2019) 6–13.

[20] Y. Li, Z.Y. Gu, T. He, X.C. Yuan, Y.Y. Zhang, Z.H.Y. Qiu, Q. Zhang, S.C. Yin, Terpyridyl-based triphenylamine derivatives with aggregation-induced emission characteristics for selective detection of Zn^{2+}, Cd^{2+} and CN^{-} ions and application in cell imaging, Dyes Pigm. 173 (2020) 107969.

[21] A. Gogoi, S. Samanta, G. Das, A benzothiazole containing CHEF based flfluorescence turn-ON sensor for Zn^{2+} and Cd^{2+} and subsequent sensing of $H_2PO_4^{-}$ and $P_4O_7^{4-}$ in physiological pH, Sens. Actuators B: Chem. 202 (2014) 788–794.

[22] F.J. Huo, Q. Wu, Q. Kang, Y.B. Zhang, C.X. Yin, A specific fluorescent probe for zinc ion based on thymolphthalein and it's application in living cells, Sens. Actuators B: Chem. 262 (2018) 263–269.

[23] Z.E. Chen, H. Zhang, Z. Iqbal, A new thiosemicarbazone fluorescent probe based on 9,9′-bianthracene for Hg^{2+} and Ag^{+}, Spectrochim. Acta A 215 (2019) 34–40.

[24] R. Singh, G. Das, Fluorogenic detection of Hg^{2+} and Ag^{+} ions via two mechanistically discrete signal genres: a paradigm of differentially responsive metal ion sensing, Sens. Actuators B: Chem. 258 (2018) 478–483.

[25] D.S. Lin, J.P. Lai, H. Sun, Z. Yang, Y. Zuo, A turn-on fluorescein spirolactam derivative as a high selective fluorescence probe for detection of silver ion(I) in water, Anal. Methods 6 (2014) 1517–1522.

[26] Z. Yang, M.Y. She, B. Yin, L.K. Hao, M. Obst, P. Liu, J.L. Li, Solvent-dependent turn-on probe for dual monitoring of Ag^{+} and Zn^{2+} in living biological samples, Anal. Chim. Acta 868 (2015) 53–59.

[27] F.Q. Bu, B. Zhao, W. Kan, L.M. Ding, T. Liu, L.Y. Wang, B. Song, W.B. Wang, Q.G. Deng, An ESIPT characteristic "turn-on" fluorescence sensor for Hg^{2+} with large Stokes shift and sequential "turn-off" detection of S^{2-} as well as the application in living cells, J. Photochem. Photobiol. A: Chem. 387 (2020) 112165.

[28] Y. Zhou, X.F. He, H. Chen, Y. Wang, S.Z. Xiao, N.N. Zhang, et al., An ESIPT/ICT modulation based ratiometric fluorescent probe for sensitive and selective sensing Hg^{2+}, Sens. Actuators B: Chem. 247 (2017) 626–631.

[29] C. Das, B. Pakhira, A.L. Rheingold, S.K. Chattopadhyay, Turn on ESIPT based chemosensor for histidine: application in urine analysis and live cell imaging, Inorg. Chim. Acta Rev. 482 (2018) 292–298.

[30] C.F. Sun, H. Li, H. Yin, Y.Z. Li, Y. Shi, Effects of the cyano substitution at different positions on the ESIPT properties of alizarin: a DFT/TD-DFT investigation, J. Mol. Liq. 269 (2018) 650–656.

[31] C.X. Yuan, S.Y. Li, Y.B. Wu, L.P. Lu, M.L. Zhu, Zn(II)-selective and sensitive fluorescent chemosensor based on steric constrains and inhibition of ESIPT, Sens. Actuators B: Chem. 242 (2017) 1035–1042.

[32] Z. Liu, G.P. Li, Y.N. Wang, J.L. Li, Y. Mi, D.P. Zou, T.S. Li, Y.J. Wu, Quinoline-based ratiometric flfluorescent probe for detection of physiological pH changes in aqueous solution and living cells, Talanta 192 (2019) 6–13.

[33] W.Y. Feng, S.Y. Gong, E.B. Zhou, X.Y. Yin, G.Q. Feng, Readily prepared iminocoumarin for rapid, colorimetric and ratiometric flfluorescent detection of phosgene, Anal. Chim. Acta 1029 (2018) 97–103.

[34] A.V. Chernyshev, N.A. Voloshin, A.V. Metelitsa, V.V. Tkachev, S.M. Aldoshin, E. Solov'eva, I.A. Rostovtseva, V.I. Minkin, Metal complexes of new photochromic chelator: structure, stability and photodissociation, J. Photochem. Photobiol. A: Chem. 265 (2013) 1–9.

[35] L.Y. Chen, S.J. Park, D. Wu, H.M. Kim, J. Yooh, A two-photon ESIPT based fluorescence probe for specific detection of hypochlorite, Dyes Pigm. 158 (2018) 526–532.

[36] Y.Q. Xu, Y. Pang, Zinc binding-induced near-IR emission from excited-state intramolecular proton transfer of a bis(benzoxazole) derivative, ChemComm 46 (2010) 4070–4072.

[37] F.F. Zhou, H.Q. Wang, P.Y. Liu, Q.H. Hu, Y.Y. Wang, C. Liu, J.K. Hu, A highly selective and sensitive turn-on probe for aluminum(III) based on quinoline Schiff's base and its cell imaging, Spectrochim. Acta A 190 (2018) 104–110.

[38] M. Kumar, A. Kumar, M.S.H. Faizi, S. Kumar, M.K. Singh, S.K. Sahu, et al., A selective 'turn-on' fluorescent chemosensor for detection of Al^{3+} in aqueous medium: experimental and theoretical studies, Sens. Actuators B: Chem. 260 (2018) 888–899.

[39] S. Zeng, S.J. Li, X.J. Sun, M.Q. Li, Y.Q. Ma, Z.Y. Xing, J.L. Li, A naphthalene-quinoline based chemosensor for fluorescent "turn-on" and absorbance-ratiometric detection of Al^{3+} and its application in cells imaging, Spectrochim. Acta A 205 (2018) 276–286.

[40] X. Chen, W. Sun, Y.J. Bai, F.F. Zhang, J.X. Zhao, X.H. Ding, Novel rhodamine Schiff base type naked-eye fluorescent probe for sensing Fe^{3+} and the application in cell, Spectrochim. Acta A 191 (2018) 566–572.

[41] P. Marimuthu, A. Ramu, A ratiometric fluorescence chemosensor for Mg^{2+} ion and its live cell imaging, Sens. Actuators B: Chem. 266 (2018) 384–391.

[42] F. Zhou, Y. Sultanbawa, H. Feng, Y.L. Wang, Q.T. Meng, Y. Wang, Z.Q. Zhang, R. Zhang, A new red-emitting fluorescence probe for rapid and effective visualization of bisulfite in food samples and live animals, J. Agric. Food. Chem. 67 (15) (2018) 4375–4383, https://doi.org/10.1021/acs.jacs.8b07110.

[43] H.P. Wang, T.T. Kang, X.J. Wang, L.H. Feng, Design and synthesis of a novel tripod rhodamine derivative for trivalent metal ions detection, Sens. Actuators B: Chem. 264 (2018) 391–397.

[44] Q. Hu, W. Li, C.Q. Qin, L.T. Zeng, J.T. Hou, Rapid and visual detection of benzoyl peroxide in food by a colorimetric and ratiometric fluorescent probe, J. Agric. Food. Chem. 66 (2018) 10913–10920.

[45] Q.F. Niu, T. Sun, T.D. Li, Z.R. Guo, H. Pang, Highly sensitive and selective colorimetric/fluorescent probe with aggregation induced emission characteristics for multiple targets of copper, zinc and cyanide ions sensing and its practical application in water and food samples, Sens. Actuators B: Chem. 266 (2018) 730–734.

[46] N.I. Georgiev, M.D. Dimitrova, Y.D. Todorova, V.B. Bojinov, Synthesis, chemosensing properties and logic behaviour of a novel ratiometric 1,8-naphthalimide probe based on ICT and PET, Dyes Pigm. 131 (2016) 9–17.

[47] M. Ghosh, S. Mandal, S. Ta, D. Das, Detection and discrimination of Al^{3+} and Hg^{2+} using a single probe: nano-level determination, human breast cancer cell (MCF7) imaging, binary logic gate development and sea fish sample analysis, Sens. Actuators B: Chem. 249 (2017) 339–347.